Molecular Catalysis xxx (xxxx) xxx–xxx

Contents lists available at ScienceDirect

Molecular Catalysis

journal homepage: www.elsevier.com/locate/mcat

Editor's choice paper

Heterogeneous Fenton reaction for the treatment of ACE in residual waters of pharmacological origin using Fe-SBA-15 nanocomposites

Tamara B. Benzaquén, Pablo A. Ochoa Rodriguez, Analía L. Cánepa, Sandra G. Casuscelli, Verónica R. Elías, Griselda A. Eimer*

Centro de Investigación y Tecnología Química (CITeQ) (UTN-CONICET), Maestro López esq. Cruz Roja Argentina, Ciudad Universitaria, Córdoba, 5016ZAA, Argentina

ARTICLE INFO

Keywords:
Acetaminophen
Drugs degradation
Heterogeneous Fenton reaction
Fe-SBA-15

ABSTRACT

SBA-15 nanocomposites were synthesized using different sources of iron by direct hydrothermal synthesis. Various characterization techniques including X Ray Diffraction (XRD) at low and high angle, UV–vis diffuse reflectance spectra (UV–vis DRs) and Temperature Programmed Reduction (TPR) were conducted. The metal speciation in the solids was different depending on the used source of iron.

The synthesized materials were evaluated in a heterogeneous Fenton process applied to the degradation of aqueous solutions of a commercial drug, acetaminophen (ACE). The catalyst synthesized with ferric sulphate showed the best activity which can be attributed to the presence of more isolated Fe^{3+} ions stabilized and accessible to reactant molecules.

Using the best catalyst, the influence of pH, catalyst initial concentration and temperature on the pollutant degradation process was studied. A maximum degradation (90.8% in a reaction time of 120 min) was achieved with an initial catalyst concentration of 1000 mg L^{-1} at pH = 4.5 and 30 °C. In addition, under these conditions iron species leaching from the catalyst was very low, ensuring the heterogeneity of reaction, stability and possibility of catalyst reuse. Finally, this method may be very effective for pharmaceutical effluent treatment and be used in the acetaminophen industry.

1. Introduction

The pharmaceutical Industry is an area of continuous growth in Argentina. Its turnover grew 250% in the last decade and its participation in the GDP (Gross Domestic Product) is around 1%. Thus, Argentina is among the leading countries in the world, with a large percentage of medicines (50%) produced by National Capital companies. In addition, this industry, which is one of the most value-added in the market, represents 5% of the total exports of country [1].

The pollution of the environment by drug residues is a constant phenomenon. Excretion, along with uncontrolled discharging during the manufacturing, inadequate disposition of effluents or waste and disposal of surplus medicines from homes and veterinary applications, are the main ways by which pharmaceutical products are carried to the water bodies [2]. The medicines are pharmacologically active substances designed for a specific action. When they reach the bodies of water, by different ways, the conventional treatment that the purification plants generally apply, are not efficient enough to remove it in their totality and as a result, these substances reach the drinking water causing long-term adverse effects [3–5].

Acetaminophen (ACE, N-(4-hydroxiphenyl)acetamide)) is one of the best-selling drugs in Argentina, because it is widely used as an analgesic, anti-inflammatory and antipyretic. Although, it has been found in European wastewater treatment plants in concentration of 6 μg L^{-1}, high concentrations (between 0.08 and 13.8 mg L^{-1}) have been described in the literature for different effluents [6]. In addition, its transformation into toxic compounds during chlorination in wastewater treatment plants has been well described by Bedner and Maccrehan [7]. Considering the potential impacts of this pharmaceutical product, their removal from wastewater before discharge is highly recommended.

In this context, alternative treatment technologies should be considered. In recent years, considerable interest has been directed toward the application of advanced oxidation processes (AOPs) for the removal of this type of pharmaceutical contaminants from water [8,9]. The AOPs, involve the generation of highly reactive chemical species (•OH) capable of oxidizing a wide variety of organic compounds.

Within AOPs, the Fenton process generates these radical species through the use of iron and hydrogen peroxide (H_2O_2) as an oxidizing

* Corresponding author.
E-mail address: geimer@frc.utn.edu.ar (G.A. Eimer).

https://doi.org/10.1016/j.mcat.2018.11.010
Received 30 July 2018; Received in revised form 14 November 2018; Accepted 19 November 2018

agent. This process is well known as an environmentally compatible alternative to improve the biodegradability of a recalcitrant wastewater [10–12], generating H_2O and O_2 on by products [13].

On the other hand, having objective the development of new sustainable processes, researchers from around the world have been making efforts for a long time to change the catalytic systems conventionally in homogenous phase by its peers in heterogeneous phase. Because it well knows, the homogeneous Fenton oxidation suffers from a few drawbacks [14–16]. To overcome these drawbacks an adequate solution seems to be the use of heterogeneous catalysts in the so-called heterogeneous Fenton-like oxidation, which also might avoid the initial acidification.

The mesoporous silicates with long-range structural arrangements, such us molecular sieves SBA-15, are emerging as interesting alternatives for the development of these heterogeneous catalysts. The most interesting of these sieves is the versatility they present for the functionalization according to the activity for which they are designed. There are lots of reports where modified silicates are synthesized for their application in the fields of absorption, catalysis and separation among others [17,18]. Particularly, the synthesis of mesoporous materials modified with the (Fe) iron is interesting because this metal can give the material a series of unique properties. Therefore, with the aim of developing materials with high catalytic performance, it's very interesting to incorporate highly stable iron species on the surface of SBA-15 type sieves.

The Fenton process has several advantages compared with others AOPs such as the hydrogen peroxide is readily available, simple to store, safe to handle, and non-aggressive to the environment. Moreover, the heterogeneous Fenton process provides an easy separation and recovery of the catalyst from the treated wastewater. Because of this, these immobilized Fenton systems provide the possibility of working in a wider pH range. Thus, obvious technological and environmental benefits [19,20] for this AOP include a net cost reduction of the treatment process and furthermore, it is not necessary to employ an energy source in the process, a fact that can further reduce the operational cost of the treatment.

Therefore, contemplating that this process does not require light, it could be feasible to support these materials in monolithic structures [21], in order to implement a continuous process with the industrial advantages that this entails. This contribute to optimize production processes and achieving an economic and environmental sustainability

Thus, in this work we propose to synthesize molecular sieves of type SBA-15 and modify those using different sources of Fe in order to study their catalytic activity in heterogeneous Fenton oxidation processes. In this way, we analysed the distribution of the metallic species generated on the solids as a function of the different sources of Fe and correlated it with their catalytic behaviour. Then, taking the most active material, the optimization of the main variables of the Fenton reaction system on heterogeneous phase (catalyst amount, pH and temperature) was carried out. For this, the degradation of a complex organic molecule difficult to biodegrade and usually found in industrial and domestic effluents, such as acetaminophen, was considered.

2. Materials and methods

2.1. Synthesis

Fe modified SBA-15 molecular sieves were synthesized by direct incorporation of metal precursor in the synthesis gel. Pluronic P123 was used as the structure-directing agent, which was dissolved in a 2 M HCl solution under stirring at 40 °C. Then, the iron precursor, $FeCl_3.6H_2O$ or $Fe_2(SO_4)_3.xH_2O$ was added to the solution following the Si/Fe molar ratio of 20 and the stirring was maintained for 30 min. Then silicon source, tetraethoxysilane (TEOS), was added dropwise to this solution and kept under stirring at 40 °C for 4 h. The pH of this mixture was adjusted to 3.5 with an aqueous ammonia solution (30 wt. %). After the pH stabilization the stirring was maintained 30 min and then the gel was aged without stirring at 40 °C for 20 h and at 80 °C for 48 h. The obtained solid was recovered, washed and dried at 60 °C. Finally, the organic template was removed submitting the solid to a calcination process (heating rate 1 °C/min until 500 °C, maintaining this temperature for 8 h). The materials were named: Fe-SBA-15(20)$_x$, where 20 is the Si/Fe molar ratio and "x" indicates the incorporated metal precursor. For comparative purposes the pure SBA-15 was synthetized following the same procedure, but without incorporation of metal source and without the step of pH adjustment.

2.2. Chemicals

Acetaminophen ($C_8H_9NO_2$, ≥ 99%, Sigma-Aldrich) was employed as the model pollutant. The experiments were performed employing reagent-grade hydrogen peroxide (H_2O_2, 30% w/v, Ciccarelli p.a.) and concentrated sulphuric acid (95–98% Pro-analysis, Ciccarelli p.a.) for pH adjustment. The treated solutions were neutralized by NaOH (reagent grade, Ciccarelli p.a.) and methanol purchased from Carlo Erba (RPE) was employed as a quenching solution. Analytical standards for chromatography analyses were purchased from Sigma-Aldrich.

2.3. Experimental setup and procedure

ACE degradation was performed in an isothermal cylindrical batch reactor. A scheme of the experimental device is shown in Fig. 1. The system included a magnetic stirring to provide good mixing conditions and to ensure the adequate suspension of the catalyst in the reaction medium. Also, the experimental setup had a thermostatic bath connected to a temperature controller to keep the temperature constant during the reaction, a liquid sampling device, a thermometer and a pH control. Finally, the entire system was covered to obtain the darkness required in the Fenton reaction.

Experimental runs began when the suspended catalyst in ACE aqueous solution was stirred, for 60 min in order to reach the adsorption/desorption equilibrium. Previously, sulphuric acid is added to adjust the pH of the medium to the desired value. After this adsorption period, the required amount of H_2O_2 solution as oxidizing agent was added and the first sample was withdrawn (reaction time equal to zero) to start the Fenton reaction. It should be noted that, in all the cases, adsorption less than 10% of ACE was observed on the solid catalyst.

The suspension volume employed in all of the experiments was 0.25 L. Runs lasted 240 min, and liquid samples were taken at equal time intervals. The measured pH of the suspension was evaluated experimentally so that this value remains almost constant throughout the runs. The experimental runs were performed at different temperatures (20 °C and 30 °C). The initial concentration of the pollutant was 20 mg L^{-1}, which is the value expected in wastewater to be treated. The stoichiometric amount of H_2O_2 required for the total oxidation of acetaminophen was calculated based on the following equation:

$$C_8H_9NO_2 + 21H_2O_2 \rightarrow 8CO_2 + HNO_3 + 25H_2O$$

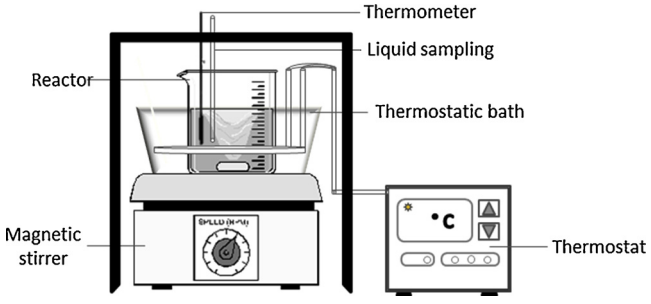

Fig. 1. Diagram of reaction system.

The degradation percentage, as the criteria of process efficiency, was calculated by Eq. (1).

$$Degradation\ (\%) = \frac{C_{ACE}^{t_0} - C_{ACE}^{tf}}{C_{ACE}^{0}} \times 100 \quad (1)$$

Where $C_{ACE}^{t_0}$ and C_{ACE}^{tf} are the ACE concentration at initial (t_0, after adsorption desorption equilibrium) and final time (t_f), respectively, (mg L^{-1}). Then, with the purpose of considering the mineralization of the commercial drug, the conversion of the total organic carbon (TOC) should be evaluated (Eq. (2)).

$$Mineralization\ (\%) = \frac{TOC^{t_0} - TOC^{tf}}{TOC^{t_0}} \times 100 \quad (2)$$

Here *TOC* represents the concentration of the total organic carbon as a function of time.

The goal is to achieve a total degradation of acetaminophen and the higher possible mineralization.

2.4. Analysis of aqueous solution samples

Samples were taken at equidistant time intervals and pre-filtered through 0.22 μm syringe filters (25 mm, Millipore). The concentration of ACE was determined using an HPLC (Perkin Elmer) with a UV–vis detector (Series 200) at detection wavelength of 242 nm A reverse phase column (Waters, C-18) was used with an isocratic mixture of acetonitrile (60%) and water (40%) as the mobile phase (flow rate 1 mL min^{-1}) at a temperature of 30 °C. The limit of detection (LoD) for ACE was determined to be 1.05 mg L^{-1}. The hydrogen peroxide concentration was analysed with a modified iodimetric technique [22] using a UV–VIS Jasco V-650 at 350 nm. To evaluate Fe leaching, the concentration of dissolved iron was measured in the final solution after filtration, by a standard spectrophotometric technique (absorbance measurements of the Fe^{2+}-phenanthroline complex at 510 nm [23]). Samples for total iron determination were first treated with ascorbic acid. The mineralization of the pollutant was monitored by measuring the total organic carbon (TOC) by direct injection of filtered samples into a SHIMADZU TOC-5050 analyser). The limit of detection (LoD) for TOC was determined to be 2.01 mg L^{-1}

2.5. Characterization of the iron oxide catalysts

The mesoporous silicates were characterized by X-Ray Diffraction (XRD) at low and high angle using a PANalytical X'Pert Pro diffractometer with Cu Kα radiation (λ = 1.5418 Å) in the range of 0.5-3° and 20-80°. The specific surface at one point was determined from N_2 adsorption measurement using a Micromeritics Pulse Chemisorb 2700, applying the Brunauer-Emmett-Teller (BET). UV–vis diffuse reflectance spectra (UV–vis DRs) were recorded using a Jasco 650 spectrometer with an integrating sphere in the wavelength range of 200–900 nm. The iron content was determined by applying the o-phenanthroline colorimetric method (3500-Fe) by spectrophotometry at 510 nm [(3500-Fe D) [24]. The method consists of the sensitivity of o-phenathroline to form a complex with the Fe^{2+} ions present in solution. Thus, the absorption at 510 nm is proportional to the concentration of solubilized Fe^{2+} ions. Previous to this analysis the solids were digested with acids, and the solutions of each sample were measured to determine the iron concentration. The reducibility of metal species developed in the solids was analysed by Temperature Programmed Reduction (TPR) experiments in the Micromeritic ChemiSorb 2720 Instruments. In these experiments, the samples were heated from 25 to 800 °C at a rate of 10 °C min^{-1} in the presence of 5% H_2/N_2 gas mixture (25 mL min^{-1} STP), and the reduction reaction was monitored by the H_2 consumption with a built-in thermal conductivity detector (TCD).

XPS (X-ray photoelectron spectroscopy) analyzes were performed on a computer equipped with a Multitechnique Specs Dual X-ray source Mg/Al model XR50 and hemispherical analyzer 150 PHOIBOS Fixed transmission mode analyzer (FAT). Spectra were obtained with a power passage of 30 eV and Al anode operated at 100 and 150 W when conditions in the main chamber were adequate. The pressure during the measurement was less than 2.10–8 mbar.

Table 1
Chemical composition and specific Surface of synthetized materials.

Catalyst	Surface (m^2/g)	Fe content (wt. %)
SBA-15	839	–
Fe-SBA-15(20)$_{Fe2(SO4)3}$	801	3.49
Fe-SBA-15(20)$_{FeCl3}$	705	4.28

3. Results and discussion

3.1. Characterization of iron catalysts

Table 1 shows the Fe content and the specific surface for the synthetized samples. It can be observed a higher metal incorporation for the sample modified with ferric chloride as the metal precursor. This sample also shows the higher decrease in the surface with respect to the pure SBA-15, probably attributed to the presence of metal species which could be blocking some pore mouths.

Low angle XRD patterns are shown in Fig. 2A. Peaks corresponding to diffraction planes usually assigned to hexagonal pore arrangement are observed, evidencing the good structural order present in all samples. For its part, the lack of peaks assignable to an iron crystalline phase in the high angle XRD patterns (Fig. 2B) indicates that the developed metal species would be amorphous or have a size under the detection limit of the XRD technique.

In order to analyse the influence of the used metal precursor on the metal species developed in the SBA-15 mesoporous structures, UV–vis DR spectroscopy was applied (Fig. 3). As it was previously reported [25,26] the obtained spectra correspond to the absorption of three different metal species. The absorption at around 270 nm can be assigned to the O(2p) to Fe(3d) charge transfer of highly dispersed iron Fe^{3+} ions in high coordination degree with the oxygen atoms of the silicate structure. The absorption at around 360 nm also corresponds to the O to Fe transitions, but in this case, the metal ions are in lower coordination with the mesoporous structures, probably in small iron oxide nanoclusters (FeO)n formed from an oligomerization of the isolated species. Finally, the absorption at wavelengths higher than 450 nm corresponds to d-d electron pair transition of Fe ions present in iron oxide species such as nanoparticles. Nonetheless, it is important to clarify that these bigger iron oxide species (nanoparticles) have a size below the limit detection of the XRD technique and are probably present inside the mesoporous channels.

It can be observed in the spectra presented in Fig. 3 that both samples show absorption corresponding to the presence of the three mentioned species. Nonetheless, with respect to the Fe-SBA-15(20)$_{Fe2(SO4)3}$ sample, the silicate synthetized with ferric chloride, Fe-SBA-15(20)$_{FeCl3}$, show an increased absorption at wavelengths higher than 300 nm. This fact is giving account for the formation of a higher proportion of nanoclusters and bigger size iron oxide species when chloride is used as the metal precursor. Likewise, the main presence of highly dispersed Fe^{3+} ions is evidenced for Fe-SBA-15(20)$_{Fe2(SO4)3}$ sample.

Temperature Programmed Reduction (TPR) measurements were applied in order to study the reducibility of Fe species developed on the SBA-15 structures as a function of the used metal precursor. Thus, the stabilization of the Fe^{3+} ions in metal species, different interacting with the support, would result in different reduction behaviours. It is important to remark that smaller and highly dispersed metal species strongly interact with the structure, hindering their reducibility. In this

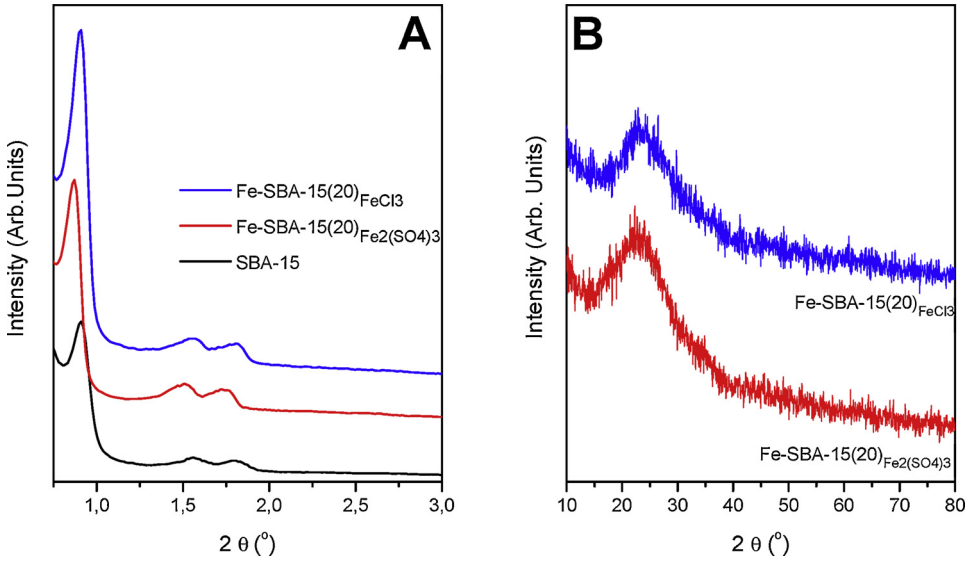

Fig. 2. XRD patterns of the synthetized solids: A) low angle and B) high angle.

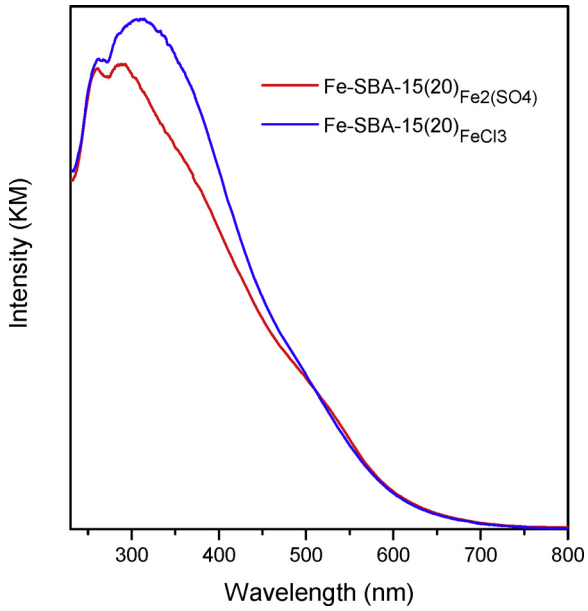

Fig. 3. UV–vis spectra of the iron modified solids.

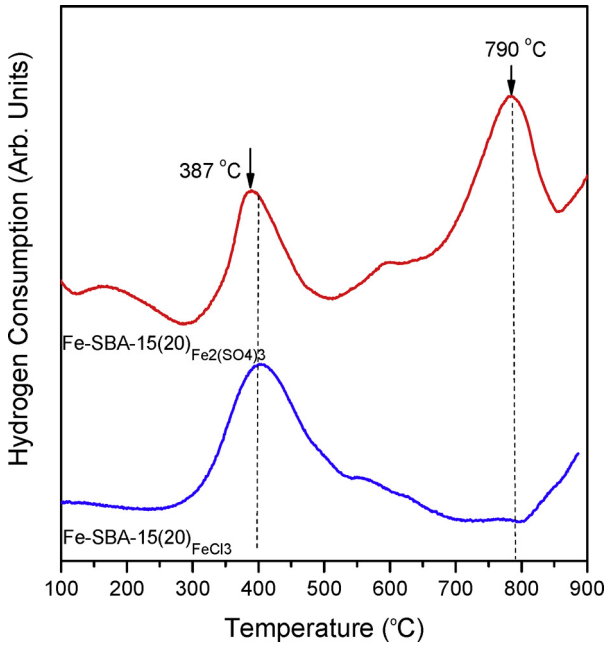

Fig. 4. TPR profiles of synthesized solids.

sense, the influence of the metal precursors in the reductive behaviours of the nanostructured silicates is evident in the TPR profiles showed in Fig. 4. The peak at low temperature (around 387 °C) observed for both samples, can be assigned to the reduction of Fe^{3+} ions present in iron oxide species. Although this H_2 consumption is due to the reduction of Fe^{3+} to $Fe^{3+/2+}$ in Fe-SBA-15(20)$_{Fe2(SO4)3}$, its broadening for the Fe-SBA-15(20)$_{FeCl3}$ sample is evidencing the further reduction of $Fe^{3+/2+}$ to Fe^{2+} and Fe^{2+} to Fe°. This easier reducibility could be due to the presence of higher size iron oxide species (nanoclusters and nanoparticles) which are formed when ferric chloride is used. It is important to note that this H_2 consumption did not corresponds to the TPR profile of bulk Fe_2O_3 evidencing that, although the oxide species formed on the silicate structure could be reduced at low temperatures, they are strongly interacting with the support and therefore only a little proportion of the Fe ions can reduce to the zero oxidation state [27]. Then, the narrower reduction peak at low temperature for Fe-SBA-15(20)$_{Fe2(SO4)3}$ sample evidences the presence of smaller size oxide species more stabilized on the structure resulting highly resistant to the reduction (Fe^{3+} ions can only be reduced to Fe^{2+}).

For this last sample, an additional H_2 consumption at around 790 °C could be observed. This peak could be associated to the presence of isolated Fe^{3+} ions bearing multiple surface oxygen bridged bonds [28]. According to Arenas et al. the reducibility of these species depends upon the number of "Fe-O-Si" linkages with the support in their first coordinative shell [28]. Thus, when the sulphate source is used, the observed peak at high temperature suggests a high degree of coordinative saturation of the isolated Fe^{3+} ions with the support, resulting them hardly reducible (790 °C). In the case of Fe-SBA-15(20)$_{FeCl3}$, the lack of this peak evidences the higher accessibility and predominance of bigger oxide species such as nanoparticles and nanoclusters. This fact does not mean the absence of the isolated species in this sample, but larger species could be hindering the access to them.

In order to complement the analysis about the metal species developed on the surface of the mesoporous silicates synthetized in this work, XPS spectra were measured. The spectra were analyzed with the CasaXPS (Casa Software Ltd, UK) software [29] and were calibrated

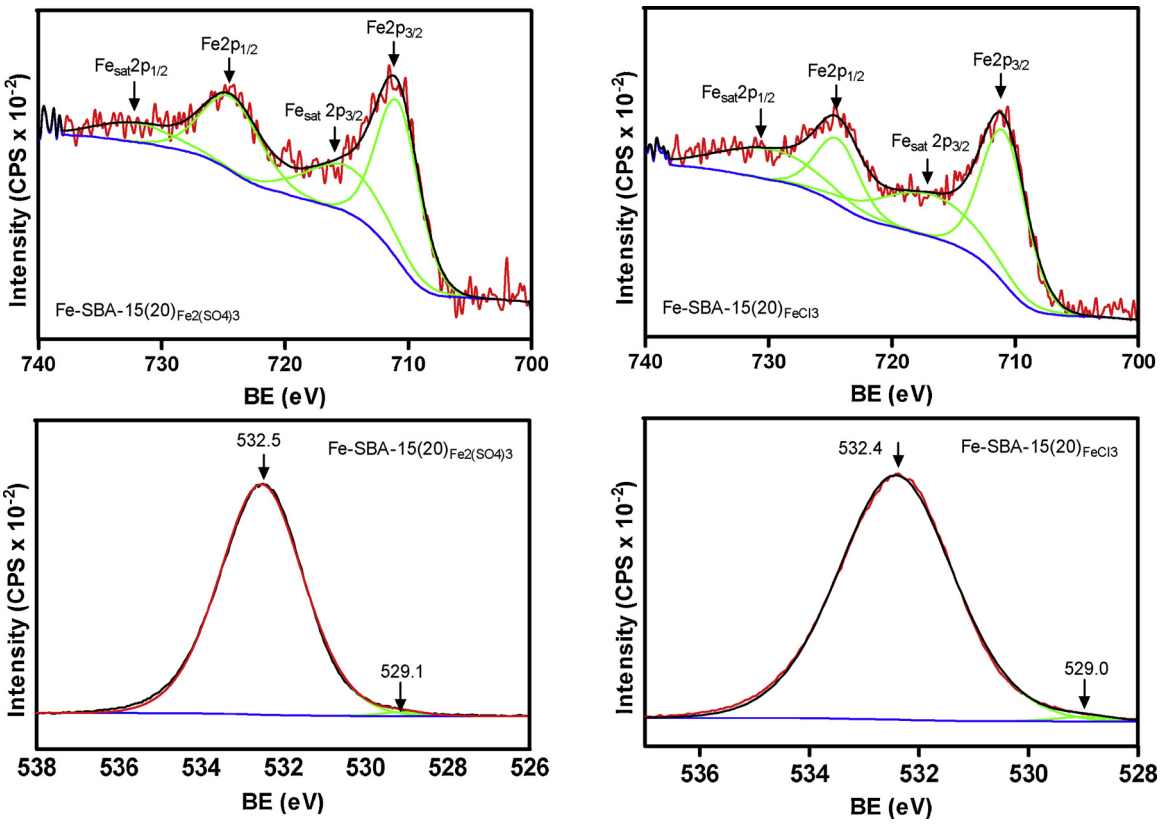

Fig. 5. XPS spectra of Fe 2p core level and O 1 s for the synthetized samples.

Table 2
XPS binding energy (BE) values and surface atomic iron concentrations for Fe-SBA-15(20)$_x$ samples.

Samples	Fe $2_{p3/2}$ (eV)	Satellite Fe $2_{p3/2}$ (eV)	Fe $2_{p1/2}$ (eV)	Satellite Fe $2_{p1/2}$ (eV)	O 1 s (eV)[a]		at.% Fe (XPS)	Surface Fe/Si (XPS)	Bulk Fe/Si[b] (AA)
					O-Fe	O-Si			
Fe-SBA-15(20)$_{Fe2(SO4)3}$	710.8	715.0	724.3	732.1	529.1(0.92)	532.5 (99.08)	0.4	0.006	0.039
Fe-SBA-15(20) $_{FeCl3}$	710.9	716.8	724.4	729.8	529.0(0.96)	532.4 (99.04)	0.5	0.007	0.048

[a] Between brackets figure the corresponding species percentage.
[b] Determined by colorimetry.

using the C1 s peak correction. The peak areas were determined using Shirley background integration and were considered as a mixed of Gaussian and Lorenztian functions. The spectra in the Fe 2p region were fitted with four peaks assigned to the Fe^{3+} chemical state (Fig. 5). As it can be observed, due to the relative low concentration of Fe in the samples, the XPS signals in this region are relatively low. Thus, it is frequently that, with respect to the bulk oxides, the XPS spectra of the mesoporous solids show wider peaks. This is taken as an evidence of the dispersion of the metal species developed on the mesoporous structures. Table 2 presents the data obtained from the spectra fitting. For both samples, two peaks emerge at around 710 eV and 724 eV corresponding to the binding energies of the Fe $2p_{3/2}$ and Fe $2p_{1/2}$, respectively. For the bulk hematite oxide, the Fe $2p_{3/2}$ peak is usually accompanied for a satellite signal at around 718 eV. In the Fe modified mesoporous samples synthetized in this work, this satellite emerge at a lower binding energy (around 715 eV). This shift would be indicating that, although the Fe^{3+} are in an oxide environment [26], the developed species not correspond to the bulk oxide. In this sense, some reports indicate that the difference in energy separation between the main peak Fe $2p_{3/2}$ and its satellite decreases when the electronegativity of the ligands decreases [30]. Then, when the metal center is lower coordinated to other Fe ions, the electron density surrounding it increases and lower energy is needed for the 3d electron promotion. In addition, these authors also assigned the mentioned binding energy (715 eV) to the presence of lower coordinated Fe^{3+} ions present in the surface. Therefore, the peaks observed in the spectra of both samples are according to the presence of isolated Fe^{3+} cations linked to surface O atoms or present in small clusters. Nonetheless, the shift to a higher binding energy for the satellite peak in the XPS spectrum of Fe-SBA-15(20)$_{FeCl3}$ (716.8 eV) gives account for an increased polymerization of the mentioned Fe species when ferric chloride was the metal precursor. On the other hand, for both samples the oxygen signal corresponding to the O1 s binding energy, could be fitted with two contributions at around 529 and 532 eV which belong to the oxygen atoms from iron species and SiO_2, respectively. In Table 2 it can be observed, the higher area percentage of the O1 s contribution corresponding to SiO_2 and only a slight contribution from the iron species. Then, although it could be possible to infer the presence of Fe^{3+} in oxide environment, a notable preponderance of oxygen from the silica matrix is seen. Nevertheless, a slight higher contribution of O from the iron species was observed for sample modified with ferric chloride, evidencing the major presence of the iron species on the surface of this sample. In this sense, Table 2 reports the surface Fe/Si atomic ratios from XPS for both samples obtained from the original spectra fitted. As the Fe/Si ratio could be considered as an indicative of the metal dispersion on the support [31], the notable lower Fe/Si atomic surface ratio with respect to the bulk

Table 3
Catalytic activity of materials synthesized from two Fe sources at different pH[a].

Catalysts	pH	ACE degradation (%)(*)	ACE mineralization (%)(**)	H_2O_2 consumption (%)(*)
Fe-SBA-15(20)$_{FeCl3}$	3.5	12.9	< 2	15.7
Fe-SBA-15(20)$_{Fe2(SO4)3}$		95.3	89.3	38.7
Fe-SBA-15(20)$_{FeCl3}$	4.5	10.5	< 2	9.4
Fe-SBA-15(20)$_{Fe2(SO4)3}$		90.8	64.0	19.2
Fe-SBA-15(20)$_{FeCl3}$	5.5	< 1	< 2	5.7
Fe-SBA-15(20)$_{Fe2(SO4)3}$		17.2	< 2	10.1

[a] C°_{CAT} = 1000 mg L^{-1} and C°_{H2O2} = 95 mg L^{-1}, at 30 °C. (*) Reaction time 120 min. (**) Reaction time 240 min.

Fe/Si ratio can be considered as a further evidence of the iron species incorporation inside the mesopores.

Considering the solids characterization results exposed it could be inferred the presence of different iron species as a function of the used iron precursor. Although, under the synthesis conditions, both metal sources provoke the formation of small size species that are not evidenced by XRD, these have different interaction with the support resulting in different reduction behaviour. In order to explain this behaviour, it should be considered that the nature of the counterions can strongly control the mechanism of nucleation and growth of oligomers during hydrolysis. In the first steps of the Fe-SBA-15(20)x synthesis, the Fe ions are in aqueous solution as hexa-aquo complexes $(Fe(H_2O)_6)^{3+}$ which have a strong tendency to hydrolyse. Then, the different nature of the anions presents in the metal precursors (size and charge) can affect the polymerization process of Fe^{3+} ions, influencing notably on the type of metal species developed on the silicate structure [32]. It is known that the use of ferric chloride, due to the small size of Cl^-, favours the polymerization in the stage of the precursor hydrolysis by the coordination of the counterions with the Fe^{3+} centres [33–37]. Thus, the formation of an intermediate polycation of 24 iron atoms has been reported during the hydrolysis when ferric chloride was used [32,37,38]. In contrast, due to their increased size, anions such as $(SO_4)^{2-}$ have a low coordination ability. Then, although each Fe atom that is surrounded by six oxygens (from the H_2O molecules) has all the potential binding sites available, in presence of such anion, this monomer only has the possibility to bind one or two Fe through corners. Therefore, the resulting structures include single-corner bonds. In fact, it has been reported a more chaotic nature for the polymerization when bigger anions are present, provoking the formation of a variety of different subunits that finally would result in the formation of smaller size iron species [32]. Therefore, the nature of the counterion would be the responsible for the presence of smaller size iron species in the silicate modified with the ferric sulphate, and bigger size species developed for the solid synthetized from ferric chloride.

Finally, the applied direct synthesis method allows the development of iron species finely dispersed on SBA-15 structure and the different metal precursors strongly affected on the nature of these species. The ferric chloride favours the polymerization of Fe^{3+} ions and the formation of bigger iron species whose presence can hinder the accessibility to the isolated species as it was inferred by TPR and XPS. Meanwhile, when ferric sulphate is used, isolated Fe^{3+} species, evidenced by UV–vis DR and TPR, would be more accessible and available on the silica structure. The presence of the bigger size anions in the synthesis gel, permits the formation of Fe^{3+} ions coordinated with the silica framework through a higher number of Fe-O-Si bonds in their first coordination sphere. These ions would be strongly linked to silica by multiple oxygen bridge bonds increasing its stability (as inferred by TPR).

3.2. Catalytic evaluation of materials

3.2.1. Preliminary assays

Before testing the catalytic activity, a set of preliminary assays was performed. These consisted of runs using only the different catalysts (without H_2O_2) and using only H_2O_2 (without catalyst). In the blank experiments without catalyst ACE was not significantly oxidized by H_2O_2 (less than 5% conversion after 300 min). From experiments using only catalyst, ACE degradations below 10% after 300 min of treatment, were obtained.

3.2.2. Selection of iron catalyst for Fenton oxidation

The catalytic performance for two different iron modified SBA-15 solids was tested for the heterogeneous Fenton process applied in the ACE degradation. For this, certain reaction conditions were established, which were kept constant in the different tests (pH = 3.5, 4.5 and 5.5; C°_{CAT} = 1000 mg L^{-1} and C°_{H2O2} = 95 mg L^{-1}, at 30 °C) in order to compare the synthesized materials. Table 3 summarizes the results of degradation of ACE for the synthesized materials, as well as the consumption of H_2O_2 and the leaching of Fe obtained at 120 min of run.

As can be seen, the metal source in the synthesis of the solids had a marked influence on the activity of the materials. The best activity was found for the silicate synthetized with ferric sulphate as the iron precursor for all pH evaluated. Besides, an appreciable consumption of peroxide and a notable mineralization of the contaminant were reached. Conversely, using Fe-SBA-15(20)$_{FeCl3}$, the percentage of degradation of the drug was kept at values lower than 15% for the three pH evaluated, and consequently the mineralization and the consumption of hydrogen peroxide reported in these cases were negligible.

The materials activity would be highly related to the metallic species present in them. For the samples synthetized with ferric chloride source, the Fe^{3+} ions would be present in less efficient species for the generation of hydroxyl radicals, with lower degree of coordination to the structure as more segregated iron oxide species (oligomers, nanoclusters and nanoparticles). Meanwhile, the most active solid (synthetized with ferric sulphate), was the one provided with stabilized and isolated Fe^{3+} ions in higher degree of coordinative with the silica framework, which besides would be more available to the reactants molecules. Thus, it could be inferred that the more isolated Fe^{3+} ions, strongly linked to the structure through multiple oxygen bonds and more accessible to the oxidant molecules were the active sites [20].

Hence, the agglomeration of large size iron oxide species could be avoided with the presence of $Fe_2(SO_4)_3$ on the synthesis gel. This fact favours the availability, on the structure of the synthesized solid, of more isolated Fe^{3+}, which would act as active sites for the generation of hydroxyl radicals, with the consequent benefits that this produces on the performance of this catalytic system. In this way, it has been reported [39] that finely dispersed Fe^{3+} ions linked on the SBA-15 surface could react with the oxidant molecules H_2O_2, giving rise to the next reaction:

$$Fe^{3+} + H_2O_2 \rightarrow Fe^{2+} + HO_2^{\cdot} + H^+ \quad (3)$$

Then, the Fe2+ ions can react with the oxidant and regenerate the Fe^{3+}, according to:

$$Fe^{2+} + H_2O_2 \rightarrow Fe^{3+} + HO^{\cdot} + HO^- \quad (4)$$

The mentioned reactions involve the formation of free radicals responsible for the organic molecules degradation. Thus, the proposed reactions indicate that the isolated Fe^{3+} available on the surface, promoted in major proportion by the use of ferric sulphate, plays a significant role in producing active radical species ($HO^{\cdot}$ and ($HO_2^{\cdot}$)) from the decomposition of H_2O_2.

The TOC removal of ACE solution was also determined. The results (presented in Table 3) indicated that the ACE was almost completely graded at 120 min and pH = 3.5 and 4.5 and good TOC removals were

obtained after 240 min of reaction with the catalyst synthesized with $Fe_2(SO_4)_3$. This indicates that very few of the intermediate by-products remained in the solution after treatment.

3.2.3. Optimization of reaction conditions

Important factors in the optimization of Fenton's conditions include pH, temperature, and concentration of hydrogen peroxide, iron and pollutant [40]. The Fenton oxidation process was optimized in terms to achieve the complete removal of ACE using the minimum concentrations of reactants. For this propose and according to previous results, a set of experimental runs for Fenton reactions was performed, using the catalyst synthesized with ferric sulphate Fe-SBA-15(20)$_{FeCl3}$ was not selected for further investigation of reaction parameters due to its insignificant contribution to the reaction.

The parameters to be optimized were: (i) The pH. Fenton's reaction is affected remarkably by pH values. It is well known that the optimum pH for the homogeneous Fenton process is in the range between 2.8 and 3 since the generation of the hydroxyl radicals is most effective at acidic conditions [41]. Therefore, at high pH values, oxidation rate decreases [42]. The stability of the catalyst toward iron leaching is also strongly dependent of the pH of the medium. At acidic conditions the loss of metal from solid catalysts is greater. Further, neutral pH conditions are usually found in contaminated wastewater. Therefore, it is important to investigate the feasibility of applying the Fenton process for pH conditions close to neutrality. Hence, a compromise between these considerations should be held to get the maximum efficiency of the process. (ii) The initial concentration of catalyst (C°_{CAT}). With an increase in the catalyst concentration, in most cases, the rate of reaction is enhanced. This type of behaviour is expected as far as mass transfer limitations are negligible and any increase in the catalyst concentration will proportionally enhance the concentration of the active catalytic species and hence the degradation rate. (iii) The reaction temperature. This is a key factor in the efficiency of the Fenton process. Limited studies are available depicting the effect of temperature on the degradation rate. Fenton's reactions operate at room temperature but, in some cases, elevated temperature is considered one of the factors that enhanced the removal of organic compounds [43]. Moreover, some pharmaceutical production facilities produce wastewater with temperatures that can fluctuate depending on the season of the year, which may affect the efficiency of these treatments. Thus, in arid and semiarid areas, the diurnal temperature during summer can range between 25 and 40 °C (with an average close to 30 °C), and during the winter it can oscillate between 12 and 25 °C (with an average close to 20 °C). This will consequently result in variable temperatures in wastewaters compared to both winter and summer conditions.

The catalytic heterogeneous reactions with Fe-SBA-15(20)$_{Fe2(SO4)3}$ for ACE oxidation were planned, according to a three-level factorial experimental design (3^k), within the following experimental domain: (i) pH, pH = [3.5–5.5]; (ii) initial concentration of catalyst, C°_{CAT} (mg L^{-1}) = [500–1500]; and (iii) two reaction temperatures, T (°C) = [20–30], average summer and winter temperatures, respectively. These working variables were called X_1, X_2, and X_3, respectively. Table 4 presents a summary of the operating conditions and coded variables for the experimental runs.

Fig. 6 shows the degradation of ACE as a function of time with Fe-SBA-15(20)$_{Fe2(SO4)3}$ at 20 °C, for the three pH values studied with C°_{CAT} = 500 mg L^{-1}, 1000 mg L^{-1} and 1500 mg L^{-1} (Fig. 6A), B) and C), respectively), keeping the rest of the reaction variables constant. In a similar way, Fig. 7 shows the degradation of ACE as a function of time with Fe-SBA-15(20)$_{Fe2(SO4)3}$ at 30 °C.

Figures show that, for almost all conditions, a complete degradation of ACE was achieved after 240 min of oxidation. Afterward, an analysis of each parameter studied on the degradation of ACE is presented.

3.2.4. Effect of initial concentration of catalyst

The influence of the catalyst amount was investigated on ACE degradation efficiency. The results followed well known trend in Fenton process, ACE degradation to increase with the increase in catalyst concentration from 500 to 1000 mg L^{-1} because more catalyst active sites were available for hydroxylation of the $^{\bullet}OH$. Conversely, ACE degradation did not present significant differences when the initial catalyst concentration was increased to 1500 mg L^{-1}. Then, according literature [44–46] it is expected that the degradation slightly decreases upon further addition of the catalyst due to the scavenging of hydroxyl radicals or other radicals when the presence of metal species is excessive [47–49]. This behaviour was reproduced for both temperatures evaluated.

Table 4
Experimental design and experimental matrix for the degradation of the ACE.

	Experimental plan			Experimental matrix		
N°	pH	C°_{CAT} (mg L^{-1})	Temperature (°C)	X_1	X_2	X_3
1	3.5	500	20	−1	−1	0
2	3.5	1000	20	−1	0	0
3	3.5	1500	20	−1	1	0
4	4.5	500	20	0	−1	0
5	4.5	100	20	0	0	0
6	4.5	1500	20	0	1	0
7	5.5	500	20	1	−1	0
8	5.5	1000	20	1	0	0
9	5.5	1500	20	1	1	0
10	3.5	500	30	−1	−1	−1
11	3.5	1000	30	−1	0	−1
12	3.5	1500	30	−1	1	−1
13	4.5	500	30	0	−1	−1
14	4.5	1000	30	0	0	−1
15	4.5	1500	30	0	1	−1
16	5.5	500	30	1	−1	−1
17	5.5	1000	30	1	0	−1
18	5.5	1500	30	1	1	−1

3.2.5. Effect of solution pH

The effect of the initial solution pH on ACE degradation was studied. Fenton's reaction was affected remarkably by pH values. As shown in Figs. 6 and 7, high removal efficiencies of ACE were observed at pH 3.5 and 4.5, for the different initial catalyst concentrations studied. However, in all cases the removal efficiency significantly declined when the initial solution pH was 5.5. This behaviour does not change due to the variation in the temperature studied.

It should be noted that the results obtained at pH = 4.5 were very similar to those obtained at pH = 3.5 but with less iron leaching from the material (see Table 5). Accordingly, the degradation results obtained with this pH are highly encouraging. As can be seen in Table 5, at 30 °C and pH = 4.5, for C°_{CAT} = 1.000 mg L^{-1}, a pollutant degradation close to 90% at 120 min was obtained, and the iron leaching into reaction medium was less than 0.85 mg L^{-1}. A similar behaviour was obtained for a temperature of 20 °C with C°_{CAT} = 1000 mg L^{-1}, where an ACE degradation of 80.8% after 120 min of operation was reached, with a Fe leaching lower than 0.7 mg L^{-1}. Under the same conditions at pH = 3.5, very similar percentages of pollutant degradation were obtained but with a higher concentration of leached iron, promoting homogeneous Fenton reaction.

3.2.6. Effect of operating temperature

Ambient conditions can safely be used with good efficiency [50]. However, a higher temperature increases the rate of hydroxyl radicals formation as per Arrhenius law, although it also decreases the efficient utilization of hydrogen peroxide due to its accelerated decomposition into water and oxygen [51]. Thus, it is sought to verify if the degradation efficiency is affected when the temperature is increased from 20 to 30 °C.

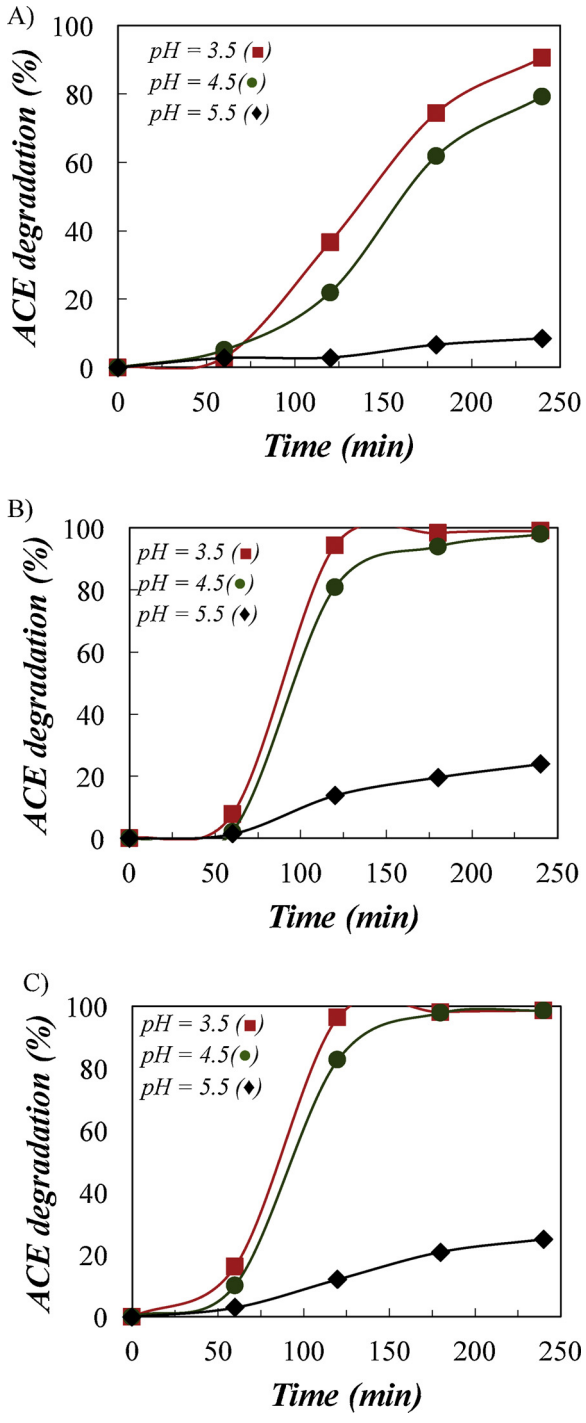

Fig. 6. Degradation of ACE as a function of the reaction time using Fe-SBA-15(20)$_{Fe2(SO4)3}$ at 20 °C and different pH, for A) C°_{CAT} = 500 mg L^{-1}, B) C°_{CAT} = 1000 mg L^{-1} and C) C°_{CAT} = 1500 mg L^{-1}.

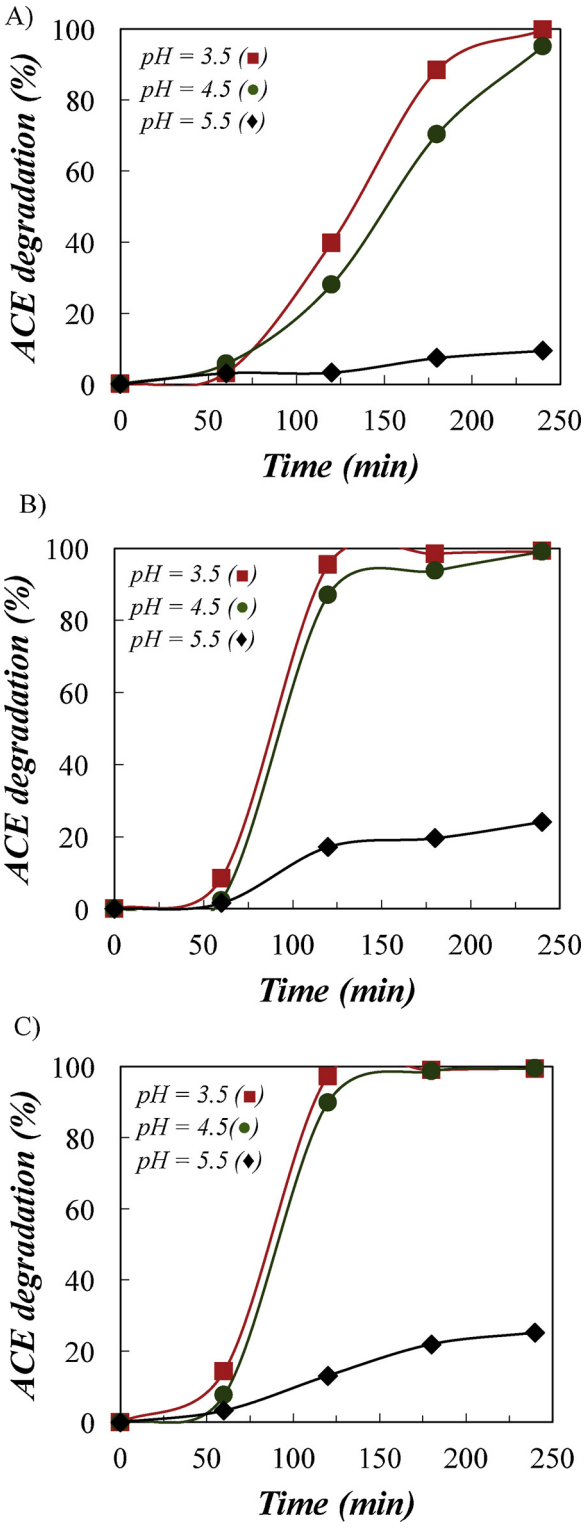

Fig. 7. Degradation of ACE as a function of the reaction time using Fe-SBA-15(20)$_{Fe2(SO4)3}$ at 30 °C and different pH for A) C°_{CAT} = 500 mg L^{-1}, B) C°_{CAT} = 1000 mg L^{-1} and C) C°_{CAT} = 1500 mg L^{-1}.

As can be seen comparing Figs. 6 and 7, the increase of temperature showed only a slightly beneficial effect for the investigated conditions. Under the more acidic condition (*pH* = 3.5), there was no significant increase in the ACE degradation when the temperature was increased from 20 to 30 °C and contaminant removal results kept constant in around 38%, 95% and 97% for C°_{CAT} = 500, 1000 and 1500 mg L^{-1} respectively, at 120 min. Meanwhile, when the pH of the medium increased to 4.5 and 5.5, increasing operating temperature had a more positive effect. The degradation of ACE improved between 10 and 15% with the increase of temperature. Beyond this temperature no significant improvement was observed, although more detailed studies should be carried onto the effect of different temperatures on this heterogeneous Fenton system.

From these results it is concluded that, for the heterogeneous photo-Fenton process, the optimal C°_{CAT}, *pH* and *T* values were 1000 mg L^{-1}, 4.5 and 30 °C, respectively.

Table 5
ACE degradation and Fe leaching in function of pH and temperature using Fe-SBA-15(20)$_{Fe2(SO4)3}$ as catalyst at C°_{CAT} = 1000 mg L^{-1} and 120 min of reaction.

pH	Temperature (°C)	ACE degradation (%)	Fe Leaching (mg L^{-1})
3.5	20	94.1	1.21
	30	95.3	1.35
4.5	20	80.8	0.65
	30	90.8	0.84

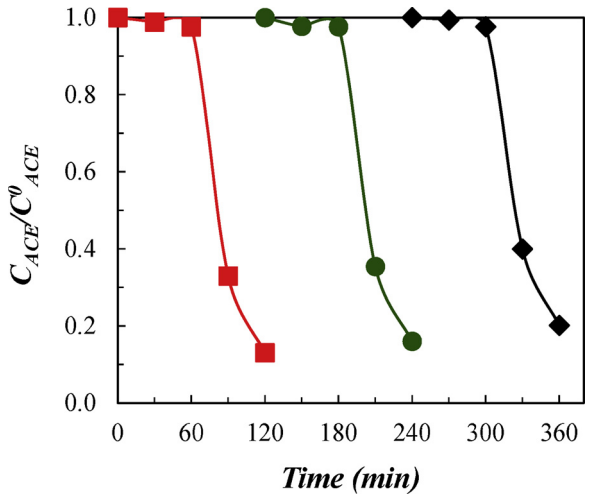

Fig. 8. Effect of regeneration of catalyst on degradation of ACE using Fe-SBA-15(20)$_{Fe2(SO4)3}$. $C^{\circ}_{CAT=}$1000 mg L^{-1}, pH = 4.5 and T = 30 °C.

3.2.7. Reuse, stability and heterogeneity of the reaction

Under the best degradation conditions obtained, reuse and leaching tests were performed in order to evaluate the catalytic stability of Fe-SBA-15(20)$_{Fe2(SO4)3}$ during successive experiments and thus its capacity of reutilization.

At the end to each catalytic cycle, the catalyst was filtered, washed, dried, and then calcined at 500 °C for 9 h, in order to remove the ACE and intermediates adsorbed. The effect of regeneration on degradation rate of ACE is shown in Fig. 8. At the end of three cycles, there was a very slight decrease in the degradation of ACE from 87% to 80%. It was likely due to the accumulation of organic intermediates on the surface of the catalyst and very slight leaching of Fe. The results suggest that even after the third regeneration the catalyst does not exhibit significant changes. In general terms, these results prove that the catalyst could be regenerated for multiple cycles.

Finally, a set of experiments in homogeneous phase were conducted to assess the efficiency of the heterogeneous process. Thus, homogeneous Fenton oxidations were performed using ferric sulphate solutions as catalyst with iron concentrations equal to the values of Fe leaching showed in Table 5 for pH = 4.5 at 20 and 30 °C. The obtained degradation values were lower than 10% for all the cases. Such feature allowed us to confirm the heterogeneity of the catalytic reaction studied.

4. Conclusions

SBA-15 molecular sieves were successfully synthetized by direct incorporation of different Fe precursors in the synthesis gel. The materials presented good structural order and high specific areas. From the analysis of UV–vis RD and TPR it can be concluded that different Fe species were developed (isolated Fe^{3+} ions, nanoclusters (FeO)n and bigger iron oxides).

The synthesized materials were evaluated in a heterogeneous Fenton process applied to the degradation of aqueous solutions of an acetaminophen. Depending on the dispersion and size of the different iron species, the nanocomposites showed different catalytic behaviours. The material synthesized with ferric sulphate, in which more isolated Fe^{3+} ions strongly linked andavailable on the surface were found, reached the highest levels of pollutant degradation.

The influence of pH, initial catalyst concentration and temperature in the heterogeneous Fenton reaction was studied using Fe-SBA-15(20)$_{Fe2(SO4)3}$. It was shown that these reaction parameters strongly influence the percentage of pollutant degradation.

The degradation value obtained with an initial catalyst concentration of 1000 mg L^{-1}, a pH = 4.5 and a temperature of 30 °C, is presented as highly encouraging given that a pollutant degradation close to 91% was obtained in a reaction time of 120 min, with a considerably low Fe leaching.

Thus, a stable and effective solid was obtained which, at pH close to neutral consumed low amounts of oxidant and provided an efficient catalytic process to degrade organic molecules, such as acetaminophen. Consequently, the heterogeneous Fenton reaction presented in this work appears as a promising pre-treatment capable to improve the biodegradability of water contaminated with recalcitrant products from the pharmaceutical industry.

Fundings

This work was supported by Consejo Interuniversitario Nacional and Consejo Nacional de Investigaciones Científicas (PDTS 231 CIN-CONICET, Resol. CE N° 1055/15-anexo 1) and Universidad Tecnológica Nacional (UTN-FRC) (MAUTICO0004427TC).

Acknowledgments

The Authors are grateful to Universidad Tecnológica Nacional (UTN-FRC) Consejo Nacional de Investigaciones Científicas (CONICET), for the financial support; and Geol. Julio Fernández for the measurements of specific area and reduction at programmed temperature of the samples.

References

[1] https://www.indec.gob.ar/.
[2] C.G. Daughton, T.A. Ternes, Environ. Health Perspect. 107 (1999) 907–938.
[3] I. Sirés, E. Brillas, Environ. Int. 40 (2012) 2012–2229.
[4] F. Yuan, C. Hu, X. Hu, J. Qu, M. Yang, Water Res. 43 (2009) 1766–1774.
[5] K. Kümmerer, J. Environ. Manage. 90 (2009) 2354–2366.
[6] M.J. Martínez Bueno, M.J. Gomez, S. Herrera, M.D. Hernando, A. Agüera, A.R. Fernández-Alba, Environ. Pollut. 164 (2012) 267–273.
[7] M. Bedner, W. Maccrehan, Environ. Sci. Technol. 40 (2006) 516–522.
[8] D.P. Mohapatra, S.K. Brar, R.D. Tyagi, P. Picard, R.Y. Surampalli, Sci. Total Environ. 470 (2014) 58–75.
[9] M. Quero-Pastor, A. Valenzuela, J.M. Quiroga, A. Acevedo, J. Environ. Manage. 137 (2014) 197–203.
[10] W. Li, V. Nanaboina, Q. Zhou, G.V. Korshin, Water Res. 46 (2012) 403–412.
[11] G.B. Ortíz de la Plata, O.M. Alfano, A.E. Cassano, J. Photochem. Photobiol. A Chem. 233 (2012) 53–59.
[12] V. Augugliaro, M. Litter, L. Palmisano, J. Soria, J. Photochem. Photobiol. C 7 (2006) 127–144.
[13] B.R. Petigara, N.V. Blough, A.C. Mignerey, Environ. Sci. Technol. 36 (2002) 639–645.
[14] M. Klavarioti, D. Mantzavinos, D. Kassinos, Environ. Int. 35 (2009) 402–417.
[15] E.V. Kuznetsova, E.N. Savinov, L.A. Vostrikova, V.N. Parmon, Appl. Catal. B 51 (2004) 165–170.
[16] T.B. Benzaquén, D.A. Barrera, P.M. Carraro, K. Sapag, O.M. Alfano, G.A. Eimer, Environ. Sci. Pollut. Res. (2018), https://doi.org/10.1007/s11356-018-2348-9).
[17] D.Y. Zhao, J.L. Feng, Q.S. Huo, N. Melosh, B.F. Fredrickson, Chmelka, G.D. Stucky, Science 279 (1998) 548–552.
[18] A. Taguchi, F. Schüth, Microporous Mesoporous Mater. 77 (2005) 1–45.
[19] S. Malato, P. Fernández-Ibáñez, M.I. Maldonado, J. Blanco, W. Gernjak, Catal. Today 147 (2009) 1–59.
[20] T.B. Benzaquén, N.I. Cuello, O.M. Alfano, G.A. Eimer, Catal. Today 296 (2017) 51–58.
[21] T. Boger, A.K. Heibel, C.M. Sorensen, Ind. Eng. Chem. Res. 43 (2004) 4602–4611.
[22] A.O. Allen, J.A. Hochanadel, J.A. Ghormley, T.W. Davis, J. Phys. Chem. 56 (1952)

575–586.
[23] APHA AWWA WEF Standard Methods for the Examination of Water and Waste Water, 19th ed., (1995).
[24] A. Greenberg, L. Clesceri, A. Eaton Wat. Pollut. Control Federation; joint editorial board. 18th ed. Washington, DC: American Public Health Association, (1992).
[25] V. Elías, E. Vaschetto, K. Sapag, M. Oliva, S. Casuscelli, G. Eimer, Catal. Today 172-1 (2011) 58–65.
[26] N. Cuello, V. Elías, M. Crivello, M. Oliva, G. Eimer, Microporous Mesoporous Mater. 203 (2015) 106–115.
[27] K. Lázár, G. Páz-Borbély, A. Szegedi, H. Beyer Studies of Surface sciences and catalysis 142 (2002) 1347-1354.
[28] F. Arena, G. Gatti, G. Martra, S. Coluccia, L. Stievano, L. Spadaro, P. Famulari, A. Parmaliana, J. Catal. 231 (2005) 365–380.
[29] N. Fairley CasaXPS Version 2.3.15 copyright 1999-2009.
[30] A. Grosnover, B. Kobe, M. Biesinger, N. McIntyre, Surf. Interface Anal. 136 (2004) 1564–1574.
[31] S. Shylesh, P. Samuel, A. Sing, Appl. Catal. A 318 (2007) 128–136.
[32] J. Rose, A. Manceau, A. Masion, J. Bottero, Langmuir 13 (1997) 3240–3246.
[33] M. Popovici, C. Savii, C. Enachea, D. Niziiansky, I. Subrt, E. Vecemikova, J. Optoelectron. Adv. Mater. 7 (5) (2005) 2753–2762.
[34] Q. Yuan, A. Yin, C. Luo, L. Sun, Y. Zhang, W. Duan, H. Liu, C. Yan, J. Am. Chem. Soc. 130 (2008) 3465–3472.
[35] C. Flynn, Chem. Rev. 84 (1984) 31–41.
[36] C. Brinker, Sol-Gel Science, Academic Press, Inc., 1990.
[37] S. Solinas, G. Piccaluga, M. Morales, C. Serna, Acta Mater. 49 (2001) 2805–2811.
[38] U. Schwertmann, J. Friedl, H. Stanjek, J. Colloid Interf. Sci. 209 (1999) 215–223.
[39] A.L. Pham, D.L. Sedlak, F.M. Doyle, Appl. Catal. B 126 (2012) 258–264.
[40] H. Zhang, H.J. Choi, C.P. Huang, J. Hazard. Mater. 125 (1-3) (2005) 166–174.
[41] D. Yang, R. Zhao, Water Pollut. 1 (2015) 167–176.
[42] B.H. Hameed, T.W. Lee, J. Hazard. Mater. 164 (2009) 468–472.
[43] M.S. Yalfani, S. Contreras, F. Medina, J. Sueiras, Appl. Catal. B: Environ. 89 (2009) 519–526.
[44] Q. Liao, J. Sun, L. Gao, Colloids Surf. A 345 (2009) 95–100.
[45] Y. Kuang, Q. Wang, Z. Chen, R. Naidu, J. Colloid Interface Sci. 410 (2013) 67–73.
[46] Y. Chen, N. Li, Y. Zhang, L. Zhang, J. Colloid Interface Sci. 422 (2014) 9–15.
[47] A.D. Bokare, W. Choi, J. Hazard. Mater. 275 (2014) 121–135.
[48] J.H. Ramirez, F.J. Maldonado-Hódar, A.F. Pérez-Cadenas, C. Moreno-Castilla, C.A. Costa, L.M. Madeira, Appl. Catal. B 75 (2007) 312–323.
[49] A. Romero, A. Santos, F. Vicente, J. Hazard. Mater. 162 (2009) 785–790.
[50] S.H. Lin, C.C. Lo, Water Res. 31 (1997) 2050–2056.
[51] A. Babuponnusami, K. Muthukumar, J. Environ. Chem. Eng. 2 (2014) 557–572.